Effect of oxidation on mechanical properties of copper nanowire: A ReaxFF (reactive force field) molecular dynamics study ⊘

Gurcan Aral ✉ ⓘD ; Md Mahbubul Islam ⓘD

Check for updates

View Online

Export Citation

CrossMark

Effect of oxidation on mechanical properties of copper nanowire: A ReaxFF (reactive force field) molecular dynamics study

Gurcan Aral[1,a)] and Md Mahbubul Islam[2]

AFFILIATIONS

[1]Department of Physics, Izmir Institute of Technology, Urla, Izmir 35430, Türkiye
[2]Department of Mechanical Engineering, Wayne State University, 5050 Anthony Wayne Drive, Detroit, Michigan 48202, USA

[a)]Author to whom correspondence should be addressed: gurcanaral@iyte.edu.tr

ABSTRACT

Nanostructures with high surface area to volume ratio, such as oxidized and coated Cu nanowires (NWs), exhibit unique mechanical properties due to their size and surface effects. Understanding the complex oxidation process of Cu NWs at nanoscale and quantifying its resulting effects on mechanical behavior and properties are significantly essential for effective usage of Cu NW devices in a wide range of applications in nanoelectronics. Here, we perform molecular dynamics simulations using ReaxFF (reactive force field) to investigate the oxidation process and mechanisms of [001]-oriented cylindrical Cu NWs and its contribution on the mechanical deformation behavior and material properties as a function of NW sizes. The relatively thin oxide Cu_xO_y layer is formed on the surface of Cu NWs in an O_2 environment, creating a core/shell (Cu/Cu_xO_y) NW structure that played a key role in governing the overall tensile mechanical deformation behavior and properties of Cu NW. The formation of oxide layer effects, including the resulting interface and defects, leads to a reduction in the initial dislocation nucleation barrier, which facilitates the onset of plasticity and stress relaxation, ultimately resulting in a negative impact on the tensile strength, Young's modulus, yield stress and strain, and flow stress when compared to pristine counterparts. It is worth noting that the tensile mechanical response and properties of the Cu NWs are highly dependent on the pre-existing oxide shell layer associated with the size of NW, determining the overall mechanical performance and properties of Cu NWs.

I. INTRODUCTION

Copper is one of the most widely used metals because of its unique properties, such as high electrical and thermal conductivities and good ductility, transmittance, high electrical and optical performance, and relatively noble characteristics.[1–6] The use of Cu as a nanowire (NW) has potential applications in the field of transparent conducting electrodes, optical sensors, and nanoelectronic devices due to superior physical and mechanical properties stemming from a high surface–volume ratio compared to their bulk counterparts.[1–4,6–16] However, the widespread applications of metallic Cu are limited due to the high chemical reactivity at ambient conditions (e.g., its poor oxidation resistance). The Cu NWs are often exposed to various reactive oxidizing environments, such as gaseous O_2 and/or water-containing medium.[1,3,6,12–14,17] In practice, the inevitable formation of a native oxide layer around the free surface of reactive metallic Cu NWs can hardly be prevented

during both bottom-up and top-down manufacture (synthesis), processing, long-term operations, and storage conditions in an O_2 environment.[1,2,5,6] Naturally, a thin oxide layer always exists inevitably on the surfaces of metallic Cu NWs with the high surface to volume ratio that can substantially change their novel surface properties, such as stability, reactivity, and corrosion behavior.[2–6,12–14] Thus, the mechanical characteristics of Cu NWs demand a thorough understanding of their oxidation process and its effects on material properties.[2,4,6,17]

The thickness of the oxide layer and the atomic structure depends on the environmental and thermo physical conditions and the NW surface properties, such as surface defects, surface orientation, stable crystal phases, morphology, and microstructure.[1,2,4–6,11–14,17,18] Thus, the oxidation process of Cu NWs typically results in the formation of an oxide shell layer with a thickness of a few nanometers with unavoidable defects.[1,4,5,11,13,14,17] Generally, the natural Cu oxide phases exist in

03 July 2023 12:42:10

the two most phases: cuprous oxide (Cu_2O) and cupric oxide (CuO), which depends on the oxidation conditions, such as oxidation temperature, exposure time, and the oxygen partial pressure.[1,4–6,11,14,17,18] Importantly, cupric oxide behaves as a more protective layer against further oxidation in electrochemical environments than cuprous oxide.[5,14] In addition, formation of the oxide-coated shell layer at the metallic Cu NWs changes surface states coupled physical and chemical properties.[2–6,11–15] For example, semiconducting, optoelectronic, and metallic properties of Cu NWs are highly dependent on the diameter, the pre-existing oxide layer, and surface defects.[2,14,15] The formation of an oxidation layer results in reduced conductivity of Cu NWs as transparent electrodes[2,12] and, thus, important to consider for their practical applications.

Furthermore, the unique properties of oxidized Cu NWs have attracted considerable interests in research communities because of its semi-conductive and electrical properties compared to their metallic counterparts.[6,11] The oxidized Cu (Cu/Cu_xO_y) NWs have various potential advantages and significant applicability in many electronics and communications devices in nano-technological applications.[2–6,11–14] The relatively large geometric surface area of the Cu NWs with and without the existence of an oxide shell layer provides abundant surface sites and allows sensor technologies to absorb more lights, leading to high efficiency and better response.[2,5,14,15] The accurate prediction mechanical properties and performance of the oxidized Cu NWs in an O_2 environment are of fundamental interest and particularly relevant for applications in different fields, e.g., nanoelectronics, sensors, catalysis, and solar cells.[1,2,5,6,11]

Importantly, the understanding of the degradation of mechanical properties and corresponding deformation behavior of oxidized Cu NWs is important for their effective and practical nanotechnological applications.[2,4,16–20] Numerous factors, including the initial structure of Cu NWs, such as the presence of impurities, structural defects, pre-existing oxide shell layer, synthesis process, morphology, and grain size, can affect the mechanical properties of Cu NWs.[2–5,7–9,12,14,16,20,21] The oxide growth rate and kinetics of the complex oxidation process of the Cu NW is rather complicated that critically depends on the types of oxidizer, ambient temperature, oxygen partial pressure, and also on the surfaces properties (surface defects, surface orientation, stable crystal phases, morphology, and microstructure).[1,4,6,17–20] These multitudes of factors that interplay with one another has a significant impact on the surface-related properties.[4,6,9,19] Thus, all these interrelated factors have resulted in diversified and contradictory findings on the oxidation mechanisms of Cu NWs and its effects on the mechanical deformation properties.[16] The high surface reactivity renders Cu NWs to be very susceptible to oxide formation; thus, the study of the mechanical deformation mechanism of pristine NW is formidable experimentally. Particularly, considering the pre-existing oxide shell layer on the surface of pristine NWs is crucial for the interpretation of experimental and theoretical results.[4] To quantify the individual contribution of the pre-existence of surface oxide layer effects on the mechanical deformation mechanism and related properties of Cu NWs is still one of the critical problems to use Cu NWs safely in nanotechnological applications.[4] In particular, the knowledge of the mechanical deformation behaviors and properties of the oxidized Cu NW is important for their niche applications in

an O_2 environment.[3,4] Furthermore, systematic computational studies under well-defined conditions to understand the influence of the presence of an oxide shell layer on the surface of Cu NW is essential to explain the contradictory observations between experimental and simulation studies.[4,17] In order to overcome these challenges, we employ ReaxFF (reactive force field) based molecular dynamics (MD) simulations to understand and quantify systematically the effect of the pre-oxide shell layer on the mechanical behavior and properties of Cu NWs. Our study reveals that the tensile mechanical deformation mechanism and properties of pristine Cu NWs in relevant diameter scales are significantly influenced by both the preexisting oxide shell layer and diameter. This combined influence leads to disproportionate effects on the initiation of dislocations for the onset of tensile plasticity, resulting in alterations to the overall mechanical deformation behaviors and properties of the pristine Cu NWs. Specifically, we found that the native oxide shell layer has a negative impact on the tensile mechanical properties, such as yield stress and strain, by providing nucleation sites for dislocations to initiate plastic deformation and by lowering the yield stress and strain in the relevant diameter of NWs, causing them to soften. This effect is particularly pronounced as the surface-to-volume ratio increases.

II. SIMULATION DETAILS

In our study, we perform MD simulations to examine atomistic mechanisms of the oxidation process of an [001]-oriented Cu NW in a molecular O_2 environment [Fig. 1] and the effect of oxidation on the tensile deformation mechanism and related properties. All atomic configurations and generated defects are visualized as well as identified using the adaptive common neighbor analysis (CNA) using the OVITO software.[22] First, NWs are prepared by creating a periodic FCC crystal of Cu with a lattice constant of 3.615 Å. Then, cylindrical [001]-oriented pristine Cu NWs with three ~4.0, ~6.0, and ~10.0 nm diameters but with the same length of ~14.9 nm along the z-direction are created by removing Cu atoms outside of a truncated cylinder radius. The three NWs contain 15 400, 34 760, and 96 360 Cu atoms with their velocities chosen from a Maxwell–Boltzmann distribution at 300 K, respectively, and the same initial un-relax length of ~14.9 nm.[23] The NWs are placed in the MD box with lengths along the z-directions. The empty region out of the created NW in the MD box is used for creating an O_2 rich environment, as seen in Fig. 1. Then, we relaxed the constructed pristine NWs using the conjugate gradient (CG) method followed by an equilibration simulation in the vacuum at a constant temperature of 300 K using a Nosé–Hoover thermostat.[24] The structural characterization of the equilibrated pristine NWs using the corresponding CNA images indicates that the structural rearrangement around the surface region causes a non-FCC structure as an unknown structure (purple color), while the rest of the Cu atoms within the NWs maintain an FCC structure (green color), as shown in Figs. 2(b) and 2(d). The circular cross section of [001]-oriented Cu NWs makes them ideal for computational purposes due to their simplicity and mechanical reliability. In recent years, [001]-oriented Cu NWs have garnered attention for their unique mechanical, electrical, optical, catalytic, and thermal properties.[1–8,11,39,43] However, their performance
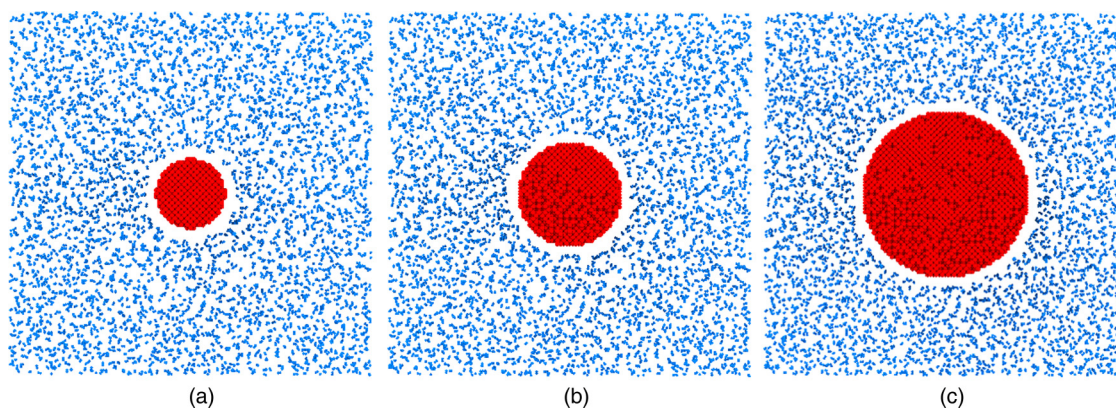
**FIG. 1.** The initial relax structure cylindrical pristine Cu NW with (a) ~2.08, (b) ~3.10, and (c) ~5.20 nm radius and ~14.9 nm length is shown from a sectional view in the O_2 molecule environment. (Red spheres represent Cu atoms, and blue spheres denote O atoms.)

depends on the pre-existing native oxide shell layer on their free surfaces. Therefore, our research focuses solely on [001]-oriented Cu NWs under tensile loading.

To study the reactivity of O_2 molecules on the cylindrical Cu free surface, we perform oxidation simulations. Followed by the equilibration of pristine NWs, 4000 O_2 molecules are randomly inserted into the enclosed vacuum region of the MD box, importantly ensuring no O_2 molecules are at least closer than 3.50 Å from

each other O_2 molecules and also at least 6.0 Å away from the nearest Cu atom. Specifically, randomly oriented and distributed 4000 O_2 molecules with their velocities chosen from a Maxwell–Boltzmann distribution at 500 K are inserted into enclosed vacuum region above the relaxed pristine Cu NW surface in the rectangular MD box.[23] Our initial physical systems are composed of a single FCC crystal structure of Cu NW and O_2 molecules, containing a total number of 15 400, 34 760, and 96 360 Cu atoms and 4000 O_2
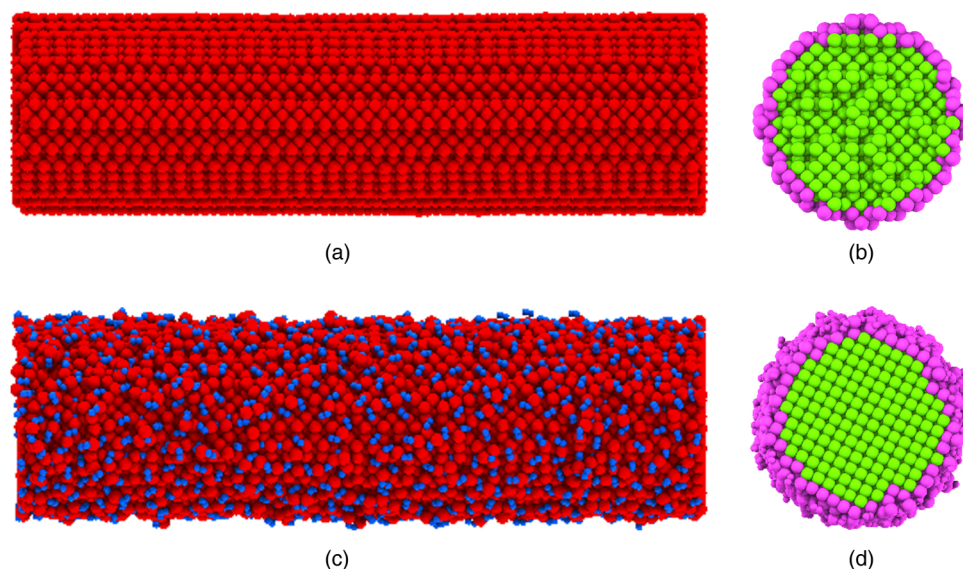
FIG. 2. The initial relax structure of (a) the pristine Cu NW with a ~2.08 radius and (c) its oxidized counterpart is shown from a side view before the applied tensile load (red spheres represent Cu atoms, and blue spheres denote O atoms), indicating a core–shell structure of a partially oxidized Cu NW. Moreover, snapshots from cross-sectional views show their corresponding local crystalline structure of (b) the pristine NW and (d) its oxidized counterpart that are determined by using CNA analysis, where the purple and green spheres represent the unknown and FCC lattice structures, respectively. Based on the CNA analysis, the overall percentage of unknown structure atoms is 22.9% and 35.6% for the pristine NWs and its oxidized counterpart, respectively.

for initial relax radii of ~2.08, ~3.10, and ~5.20 nm of the pristine NWs, respectively. The corresponding initial average number density of the O_2 molecules is approximately $5.9 \times 10^{-4}/\text{Å}^3$, which is equivalent to ~40 bar. The system consisting of the pristine Cu-NW surrounded by O_2 molecules in a gaseous atmosphere is simulated for a total of 0.5 ns. All oxidation simulations are performed at a constant temperature of 500 K using a Nosé–Hoover thermostat by applying periodic boundary conditions in all the directions.[24] The metallic Cu NW is easily oxidized within a total of 0.5 ns of time that upon exposure to relatively high O_2 pressure and temperature accelerates the oxidation process to form relatively a relatively very thin native oxide layer in a shorter time.[18] The oxidation simulations create a Cu–Cu_xO_y core–shell NW with an ~0.343 to ~0.179 nm thick amorphous oxide layer around a free surface of pristine Cu NWs [Figs. 2 and 3]. At the end of the oxidation simulation, we remove O_2 molecules from the MD box that did not interact with any Cu atoms. At the end of oxidation simulations, the total 1893, 2256, and 3181 O reacts with the surface to form a Cu_xO_y shell structure of NWs with increased NW radius, respectively. Likewise, the pristine NWs and the formation of an oxide layer lead to the destruction of the FCC crystalline structure into disordered structures around the surface layer, e.g., induce amorphization.

After creating all the NWs with and without an oxide shell layer in vacuum, they are again relaxed using the conjugate gradient (CG) method and then thermalized at a constant temperature of 300 K using a Nosé–Hoover thermostat in order to prepare them for the mechanical testing.[24] Furthermore, we equilibrate the NWs in the isothermal–isobaric (NPT) ensemble in order to relax zero pressure in the z direction with maintaining temperature at 300 K.[25] This procedure allows one to obtain a stable free surface and to relax internal stress. The NWs can freely relax radially and axially during these processes. We observed a slight expansion along the lateral free surfaces. Before the applied mechanical loads, the initial relaxed configuration for the pristine cylindrical NW and its oxidized counterpart in vacuum is shown in Fig. 2. Subsequently, to examine a possible influence of a pre-existing oxide shell layer on the mechanical deformation response and properties, we perform all deformation simulations based on the relaxed configurations of all NWs [Fig. 2(a)] by applying a uniaxial external constant tensile strain rate of $1 \times 10^8 \, s^{-1}$ along the [001] axial direction in the z-axis using the NVT ensemble at a constant temperature of 300 K.[25] In order to remove artificial end effects and mimic an infinitely long NW, a periodic boundary condition is only applied to the loading direction during mechanical deformation. The generated overall average stress vs strain is calculated from each atom using the virial theorem during the deformation process, which is corrected by the true volume of the NWs in order to obtain the engineering stress–strain curves in the [001]-oriented direction for each NW, as we used in previous MD simulations.[23,26–33] The uniaxial tensile strain is applied until reaching at ~28% elongation. Equations of motion are integrated with the velocity of the Verlet algorithm using a time step of 0.25 fs in all simulations.[23] Each atomic charge in the system is also calculated at each time step by using the electronegativity equalization method, maintaining a total charge of system zero ($\Sigma_i q_i = 0$).[34]

We used a Cu–O force field developed by van Duin and co-workers for the study.[35] We performed all our MD simulations using a large-scale atomic/molecular massively parallel simulator (LAMMPS) code.[36] More detailed information about the optimization and validation of the Cu/C/O/H ReaxFF potential parameters, including validation data on the mechanical properties of copper and its oxide systems, could be found in Ref. 35. Importantly, the training set included parameters for elastic properties, cohesive energy, lattice constant, surface energies, and vacancy formation energies, among others. This extensive training allows the ReaxFF potential to accurately predict structural properties, such as lattice constant, density, and bulk modulus, and mechanical properties of Cu NWs. In this study, we have demonstrated its capability in predicting the mechanical mechanisms and properties of Cu NWs. Briefly, in the ReaxFF formalism on MD simulations, the bond order between pairs of atoms used to define all of the connectivity-dependent interactions is calculated from the interatomic distances and also updated dynamically at every time step of the MD simulation.[34] The dynamic bond order and the charge transfer among atoms allow the method to describe complex chemical reactions and/or generation of chemical bonds, such as metallic bonds, ionic bonds, and covalent bonds.[34] ReaxFF has been successfully used for various systems, such as metallic Al, Ni, and Fe NWs to obtain insight into the oxidation of reactive complex materials and its responsible impact on degradation of mechanical deformation performance and predict related physical and chemical properties.[17,26–33] Furthermore, these previous studies revealed that oxidized metallic NWs exhibit to have unique mechanical properties, which depends on several factors, such as the oxide shell layer thickness, the local structure of the oxide shell layer with the combined effect of the externally applied mechanical loads, determining the overall stress–strain behaviors in the NWs and the deformation mechanism and properties.

III. RESULTS AND DISCUSSION

A. Oxidation of metallic Cu NWs in an O_2 environment and characteristics of the core/shell (Cu/Cu_xO_y) structure

In order to systematically study the effect of the oxide layer on the mechanical properties of NW, we first perform the oxidation simulations to investigate the initial dynamical and structural properties of the oxidation process of the cylindrical [001]-oriented metallic Cu NW with three different diameters in an O_2 molecular environment. We study the growth of the oxide shell layer and the local structure of the resulting metal oxide surfaces for a total of 0.5 ns. Each configuration of pristine NWs is placed at the center of the simulation box with the same initial number of 4000 O_2 contents. Then, all oxidation simulations are performed at the temperature of 500 K. Previously, Leitner *et al.* observed the important fact that the oxidation processes of 25–22 nm metallic Cu-nanoparticles (NPs) start slightly above 150 °C, indicating that the nanoscale oxidation of metallic Cu NPs is size and temperature dependent phenomena.[37]

The complex oxidation of Cu NW starts with the direct impingement of O_2 on the free surface of NW and then proceeds dynamically through adsorption and/or dissociation of O_2. However, O_2 is adsorbed at the active sites of the free surface of NW and then can partially dissociate, playing major role whole heterogeneous oxidation reactions on the pristine Cu NW surface. The

03 July 2023 12:42:10
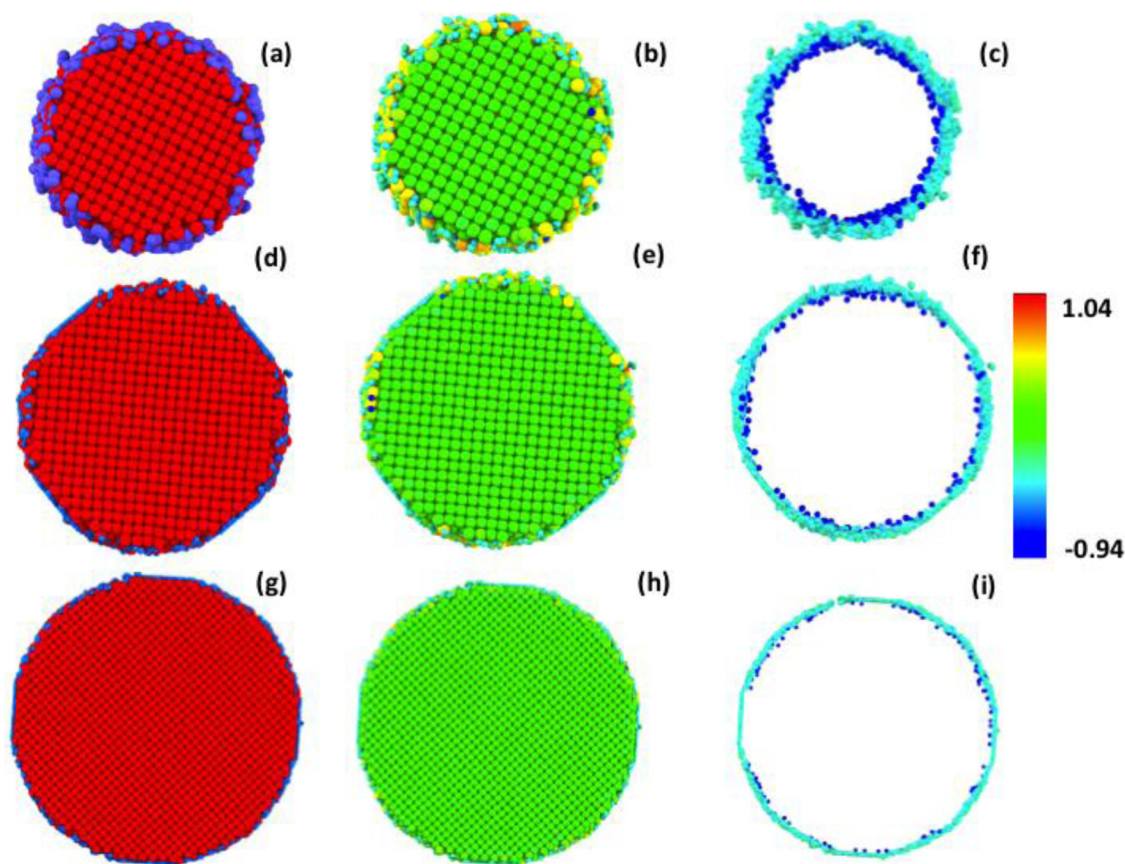
FIG. 3. Before the applied tensile load, the initial relax structure oxidized Cu NW with (a) ~2.35, (d) ~3.30, and (g) ~5.37 nm radius is shown from the front view (red spheres represent Cu atoms, and blue spheres denote O atoms), where their corresponding charge distribution of each Cu and O atom in each (b), (e), and (h) figure is colored with their atomic charge values. The charge evaluation of all atoms in the core/shell structure of NWs indicates that the Cu and O atoms are positively and negatively charged, respectively, due to the electron exchange between Cu and O atoms associated with the formation bond of a Cu–O bond, e.g., due to growth of the oxide shell layer, while keeping the charge state of Cu atoms nearly unchanged in the metallic core region. For a better presentation of the charge evaluation in the core/shell structure of NW, (c), (f), and (i) O atoms are shown entirely.

unsaturated Cu–Cu bonds on the free surface of Cu NW interact with the O_2 to reduce the surface energy of the metallic NW. The atomic charges of each atoms in the oxide Cu NW are visualized and presented in Figs. 3(b), 3(c), 3(e), 3(f), 3(h), and 3(i). These partially localized movement and diffusion of O and Cu ions through the oxide layer lead to the formation of a relatively thicker oxide shell layer and modulation of the fcc surface states of NW (structural transformations). The O and Cu peak intensity around the oxide layer has increased and decreased due to the corresponding $Cu-O_2$ and/or $Cu-O$ bonding among them and partially the inward diffusion of O atoms to the metallic core and outward diffusion of Cu atoms to a gas phase, respectively, as seen in Fig. 4.

The relatively high pressure and temperature increase the kinetic energy of atoms and the collision probability between O and Cu atoms, which contribute to overcoming the activation energy barrier and, thus, the oxidation process relatively in a shorter time. In particular, the surface atoms of NW have higher

reactivity in oxidation reactions, especially the initial stage of oxidation due to their unsaturated bonds. The oxidized Cu NWs form core–shell structures and reconstructed surface structures, including the interface between the oxide layer and the un-oxidized Cu core, as seen in Fig. 3. Upon the resulting successful oxidation process, the total 1893, 2256, and 3181 O atoms are consumed with the surface oxide shell layer as the NW radius increases, respectively, which lead to a decrease in the size of the metallic Cu core of the NWs. However, the rest of the O_2 molecules do not react with the metallic Cu NW and, therefore, not contribute to the formation of a Cu_xO_y oxide layer. Hence, we observe that the crystalline metallic Cu NW transforms gradually into a core–shell structure, which consists of a thin oxide layer and an un-oxidized metallic Cu core as a consequence of the oxidation processes.

We calculate the thickness and properties of the oxide layer from the radial density profile change of Cu and O atoms with a
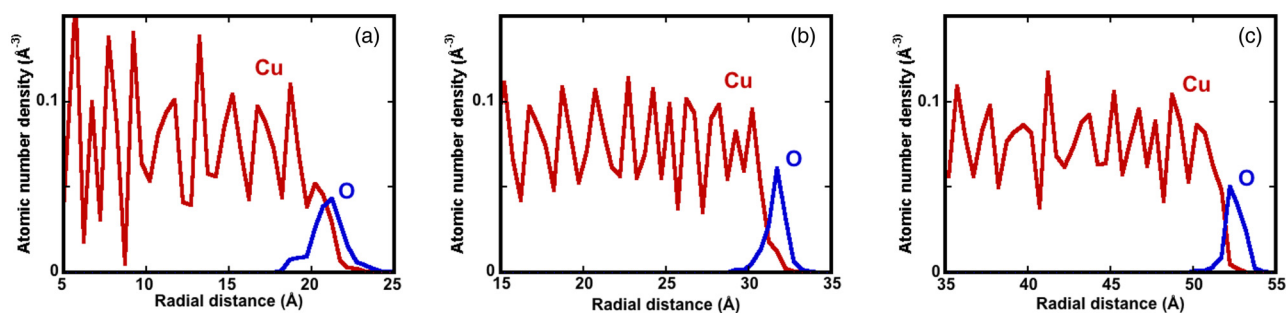
FIG. 4. The radial density profiles of Cu (red) and O (blue) atoms per unit volume for the relaxed structure of the oxidized Cu NWs with radius (a) ∼2.35, (b) ∼3.30, and (c) ∼5.37 nm, respectively, where the radial radius "*r*" is the distance from the center of NWs with respect to each radial shell width of 0.5 Å. Ionic O species penetrate slightly deeper upon the oxidation process with O_2 molecules, indicating that the Cu NWs are oxidized. Forming an oxide layer mainly present on the surface of the NWs. Notably, the density profiles reveal also that Cu atoms segregate from the metal layer into the oxide layer, and thus, the average diameter of the oxidized Cu NW expands outwardly upon the oxidation process.

0.5 Å radial width, as shown in Fig. 4. The Cu and O density peaks vary along the radial depth around the oxide that enables us to determine qualitative formation of oxidation regions, including the interface boundary and the oxide thickness based on the relative changes in the concentration of the O and Cu atoms. It indicates the oxygen concentration gradients between the O_2 environment and the metallic core and limited penetration of oxygen through the metallic surface and incorporation of the Cu–O_2 bonding around the NW free surface. Importantly, formation of Cu–O_2 bonds, e.g., relatively low dissociation of O_2, is maintaining more oxygen atoms near the surface of the Cu NWs, which modulates further oxidation. We observe a change in the morphology, shape, and relative intensities of the radial number distribution of Cu atoms as compared to the pristine counterpart. Specifically, both limited inward and outward diffusion of ions in the developing oxide layer and formation of Cu–O_2 bonding result in the change of the radial O and Cu atom concentration (density) distribution and locally change the distinct atomic arrangements and the increased growth of the thickness of the oxide layers. The successful oxide reduction around the free surface of pristine Cu is associated with the development of an oxide shell layer, which grows outward from the surface of the original metallic particle and, therefore, leads to the increase in the diameter and volume of NW. Correspondingly, the oxidized NW expands radially relative to the pristine counterpart. Specifically, the oxidation process leads to an increase in the average radius of NWs from ∼2.08, ∼3.10, and ∼5.20 nm to ∼2.35, ∼3.30, and ∼5.37 nm, respectively. Furthermore, the average inward and outward position of O and Cu ions of these peaks in the oxidized Cu NW reveals that the estimated average thicknesses of oxide Cu_xO_y shell layers are ∼0.343, ∼0.219, and ∼0.179 nm for the radii of ∼2.35, 3.30, and 5.37 nm, respectively. Importantly, these corresponding oxide layer thicknesses are approximately around the Cu–O bond length (1.91 Å) that could be consistent with many adsorbate-induced diffusion processes, involving core–shell Cu NPs.[1,11,18] Oxide shell growth contributes to the change in the surface morphology of the NW. Our results indicate that the mobility and direct impingement of O_2 into the surface is associated with the relatively high

temperature and pressure, which increase the contact probability between O_2 and the Cu NW surface and also assist chemical reactions, resulting in O_2 being absorbed and partially dissociated.

The surface of the cylindrical NWs is associated with different facets and morphology effects on the oxidation kinetics and the nucleated oxide crystal structure. Oxidation of the cylindrical Cu NW with O_2 is found to occur preferentially at some active sites on the Cu NW surface. The observation suggests that some reaction sites on the surface have higher reactivity than others. Actually, we observe a non-uniform O distribution and anisotropic oxide growth around oxidized Cu NW, which are mostly due to localized surface reorganization. The non-uniform O distribution around the Cu NW surface leads to various types of structural defects. Also, several kinds of unsaturated sites with different coordination numbers and the relatively large surface-to-volume ratio act as driving forces to expedite the reaction with oxygen in air to form an oxide layer even at low temperatures.[6] In practice, the free surface of the pristine NW is highly reactive mediated by high specific surface areas, different facet orientations, defects, imperfections, and chemical and structural heterogeneities that assist initially the adsorption and dissociation of O_2 molecules during the oxidation process.[6] Heterogeneous nucleation of the Cu–O and Cu–O_2 phase is non-uniformly distributed around Cu NW surfaces due to the cylindrical Cu NW associated with the different underlying faceting, surface areas, step edges, and the local microstructure at the NW free surface. According to the previous studies, the surface orientation of Cu crystals plays a significant role on the oxidation process, such as O diffusion into metallic core. Popovski *et al.* investigated the thermal oxidation growth process of Cu NWs for three different Cu surface orientations in an O_2 environment and also the microstructure of CuO NWs on surfaces.[14] They showed that the growth process, formation, and microstructure of CuO NWs depend on surface orientation, thickness, lengths of morphology, and temperature. For example, the nucleation density of cuprous oxide islands depends on the facets of Cu crystals; e.g., a higher oxidation nucleation density was observed on (110)-oriented Cu than on (100)-oriented Cu during the initial phase of the oxidation process.

B. Atomic local structural analysis (characterization) of the oxidized surface of NWs

We investigate the local structural properties of the oxide layer through the coordination of Cu with O atoms and the partial radial distribution functions (PRDF) and then compare the results with available experimental and theoretical data. It would provide us direct understanding of the surface oxide layer local microstructure–mechanical property relationship. Generally, the physical, chemical, and mechanical properties of Cu NWs are critically dependent on the atomistic structures of the free surfaces and subsurfaces (e.g., the surface states and/or effects), originating from the breaking of the atomistic symmetry of the initial structure sequence due to the oxidation of the cylindrical geometry of the NWs. Therefore, the structural features of the surface oxide layer are fundamentally responsible for the different mechanical deformation properties of the Cu NWs. In particular, the growth kinetics of the oxidation process predominantly governs the physical and chemical bonding, the ordering of metallic crystalline structures via local structural transformation, and also changes in the shapes, morphology, and sizes of NW. Specifically, the growth of the oxide Cu_xO_y shell layer results in the destruction of the symmetry and promotes creation of defects around the NW surface, which is possibly due to ionic interaction induced phase transformation and surface reorganization.

The PRDF provides information on the short-range atomic arrangement structure, particularly obtaining the average Cu–O, O–O, and Cu–Cu bond lengths. Figure 5 shows the radial distributions of the PRDF of Cu–O and Cu–Cu atoms for the oxidized NWs. The position of the first peak named as the first nearest neighbor distances indicates that the Cu–O bond length is around ~1.90 Å in the oxide region of 1.8–2.4 nm for the radius of ~2.35 nm, ~1.90 Å in the oxide region of 2.9–3.3 nm for the radius of ~3.30 nm, and ~1.91 Å in the oxide region of 5.0–5.4 nm for the radius of ~5.37 nm, respectively, that is consistent with earlier investigations. The Cu–Cu bond lengths in the corresponding oxidized regions are ~2.63, ~2.63, and ~2.64 Å, respectively.

Ma et al. estimated that the average Cu–O bond length is around 1.91 Å using the pair distribution function (PDF).[18] Similarly, Jeon et al. reported that the main peak of the Cu–O bond length with a slight breakdown is around 1.93 Å.[1] Ahmed et al. investigated comprehensively the structure properties of solid and melted spherical CuO NPs, such as mean Cu–O and Cu–Cu bond lengths and average coordination numbers as a function of size and temperatures by using MD studied.[11] They showed that Cu–O bond distances for both in the solid and melted phases are independent of temperature, while the Cu–O bond for solid NPs length slightly decreases with the size of NPs. The mean Cu–O bond lengths of melted NPs vary slightly with the system size between 0.191 nm (2 nm NP) and 0.193 (6 nm NP). They revealed that bulk values of Cu–Cu and Cu–O bond lengths are 0.275 and 0.194 nm for all NPs, respectively. Importantly, the Cu–Cu bond lengths are more sensitive to the size of the system than to those of the melted phase. For example, Cu–Cu nearest neighbor distances in the solid phase are 0.270 and 0.274 nm for 2 and 6 nm NP, respectively.

To further understand the resulting oxide structure, we also investigate the coordinated structures of Cu with O atoms, e.g., the coordination number with a radial cutoff distance of 2.2 Å, which is the first minimum of Cu–O PRDF. Specifically, the coordination number of O atoms around Cu atoms is computed as the distribution of the Cu–O minimum distances based on the RDF. The resulting oxidation process of Cu NW leads to CuO_n-like oxide structures. The oxidized CuO_n structures where n = 0, 1, 2, 3, and 4 are used for the number of O atoms bonded to Cu atoms to distinguish the oxide structures and describe the oxidation state of Cu NW.[18] The un-oxidized Cu atoms are expressed as CuO_0. The pristine Cu NWs with three ~2.35, ~3.30, and ~5.37 nm radius contain 15 400, 34 760, and 96 360 Cu atoms, respectively. At the end of oxidation simulations, the total numbers of the Cu atom bonded with O atoms in the form of absorbed O_2 molecules and O ions are 2344 (~15.2%), 2283 (~6.6%), and 2932 (~3.1%) for the NWs with three ~2.35, ~3.30, and ~5.37 nm radius, respectively, indicating that the rest of ~84.8%, ~93.4%, and ~96.9% of Cu atoms remain un-oxidized. The coordination of O atoms around Cu atoms all over the oxidized NW with the smallest radius is composed of CuO_1 (total number of CuO_1 = 1579), CuO_2 (total number of CuO_2 = 724), CuO_3 (total number of CuO_3 = 40), and CuO_4 (total number of CuO_4 = 1) coordinated structures. Correspondingly, the total coordination numbers for the NW with ~3.30 radius are 1942 for CuO_1, 331 for CuO_2, and 10 for CuO_3 structures and for the NW with ~5.0 radius are 2738 for CuO_1, 188 for CuO_2, and 6 for CuO_3 coordinated structures, respectively. Furthermore, the CuO_3 coordinated atoms are relatively less present in the oxide region. Interestingly, Ma et al. regarded CuO_2 and CuO_3 structure as Cu_2O-like oxide structures.[18]

To better understand the form of CuO and Cu_2O oxide structures, such as the bond between O_2 and Cu atoms on the NW surfaces, we have conducted a characterization of a short-range local microstructure of O–O atoms. This will provide more comprehensive information on the atomic structure of the oxide shell layer and the nature of bonding between Cu and O/O_2 in the CuO_x species. Figure 6 shows the calculated RDF of O–O pairs for all oxide-coated Cu NWs. The first and second peaks appear at around ~1.23 and ~1.36 A in the Cu-O RDF, which is consistent with the trend predicted based on the observation in Refs. 38–41, revealing the existence of absorbed O_2 molecules on the free surface of NW in the form of $Cu–O_2$ and mostly the form of the O–Cu–O structure. Herein, the shorter O–O distance (e.g., the first peak value) is equivalent to that of the O_2 bond length value of 1.22 Å. This gives a strong indication that the adsorption of O_2 on the reconstructed Cu NW surface occurs directly through either by the form of $Cu–O_2$ and/or the form of an O–Cu–O structure, respectively, which is consistent with experimental studies.[41] The structurally defined CuO_2 moieties have two isomers: a $Cu–O_2$ complex and an O–Cu–O (copper dioxide) structure.[39–41] Herein, the first and second peaks may correspond partially to the form of $Cu–O_2$ and mostly to the form of an O–Cu–O structure, respectively. The total 1893, 2256, and 3181 O atoms react with the metallic NW surface to form an oxide shell structure (Cu_xO_y) of NWs as the NW radius increases, respectively. The total number of O atoms incorporated with a Cu atom in the form of $Cu–O_2$ and O–Cu–O structures and O ions are 126 (~6.6), 1416 (~74.8), and 351(~18.5) for the oxidized NW with a radius of 2.35 nm, respectively. Similarly, the corresponding numbers are 126 (~5.6), 2000 (~88.7), and 130 (~5.8) for the oxidized NW with a radius of
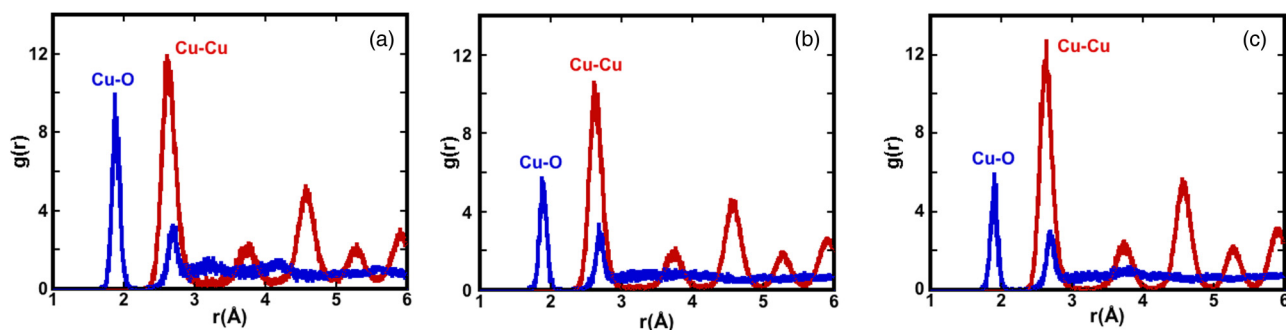
03 July 2023 12:42:10

FIG. 5. Shows the partial radial distributions (e.g., the pair distribution function) of Cu–O and Cu–Cu atoms for the oxidized NWs with radius (a) ∼2.35, (b) ∼3.30, and (c) ∼5.37 nm.

3.30 nm and 456 (∼14.3), 2620 (∼82.4), and 121 (∼3.8) for the oxidized NW with a radius of 5.37 nm. These results give us a reason to assume that that most of the O atoms are not bonded with one Cu atom to form CuO like oxide structures, indicating the fact that $Cu–O_2$ readily forms on the free surface of NWs before transformation to CuO. Jaatinen *et al.* observed that the adsorption of O_2 on the Cu surface occurs through a molecular precursor state rather than a direct dissociative process through some other

mechanism, such as a steering mediated process, depending on the oxygen coverage.[38]

Similarly, we also investigate the coordinated structures of O with Cu atoms, e.g., coordination number with a radial cutoff distance of 2.2 Å. The oxidized OCu_n structures where n = 0, 1, 2, 3, 4, 5, and 6 are used for the number of O atoms bonded to Cu atoms. The total coordination of Cu atoms around O atoms all over for the NW with 5.37 nm radius is 456 (∼17.2%) for OCu_0, 2620

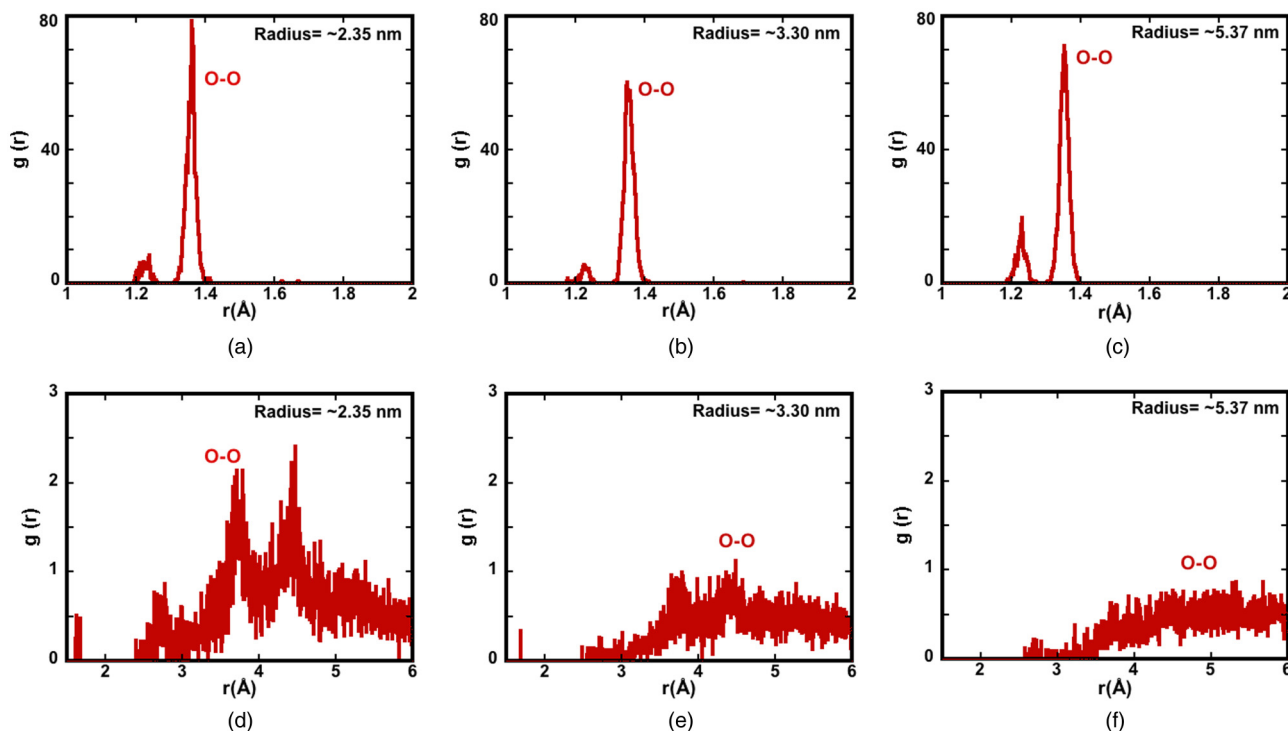**FIG. 6.** Shows the pair distribution function of O–O atoms for the oxidized NWs with radius (a) ∼2.35, (b) ∼3.30, and (c) ∼5.37 nm in the range of r = 1–2 Å and also with radius (d) ∼2.35, (e) ∼3.30, and (f) ∼5.37 nm in the range of r = 1.5–6 Å, respectively.

($\sim$82.4%) for OCu$_1$, 1 for OCu$_2$, 4 ($\sim$0.1%) for OCu$_3$, 7 ($\sim$0.2%) for OCu$_4$, 88 ($\sim$2.7%) for OCu$_5$, and 5 ($\sim$0.1%) for OCu$_6$ coordinated structures. Correspondingly, the total coordination numbers for the NW with $\sim$3.30 nm radius are 126 ($\sim$5.6%) for OCu$_0$, 2000 ($\sim$88.6%) for OCu$_1$, 2 ($\sim$0.1%) for OCu$_2$, 7 ($\sim$0.3%) for OCu$_3$, 11 ($\sim$0.5%) for OCu$_4$, 95 ($\sim$4.2%) for OCu$_5$ ($\sim$4.2%), and 15 ($\sim$0.7%) for CuO$_6$ structures. For the oxidized NW with $\sim$2.35 nm radius are 126 ($\sim$6.7%) for OCu$_o$, 1415 ($\sim$74.7%) for OCu$_1$, 6 ($\sim$0.3%) for OCu$_2$, 9 ($\sim$0.5%) for OCu$_3$, 22 ($\sim$1.7%) for OCu$_4$, 281 ($\sim$14.8%) for OCu$_5$, and 34 ($\sim$1.8%) for OCu$_6$ coordinated structures, respectively.

Our structural analysis indicated that the pristine Cu NW undergoes oxidation in an O$_2$ environment that leads to form the core–shell (Cu$_x$O$_y$) structure and the interface between the oxide layer and the un-oxidized metallic Cu core. The formation of the oxidation layer on the surface involves the structural evolution and transformation of NWs by interactions of O atoms and O$_2$ with the reactive Cu atoms around the surface. Importantly, O and O$_2$ are distributed inhomogeneously within the oxide shell layer. The cylindrical geometrical confinement effects could lead to different oxidation dynamics and result in various oxide local atomic structures and defects around the oxide layer. Particularly, the oxidation defects evolve via inward and outward ionic diffusions and local structural transformations during the oxidation process. These can explain why we observe considerable different surface oxide effects on the mechanical tensile properties of the NWs.

C. Effects of the pre-oxide shell layer on the tensile stress–strain behavior and deformation properties

In order to understand, quantify, and identify the intrinsic effects of size and the surface pre-existing oxide layer on the Cu NW surface in the tensile deformation behavior and mechanical deformation properties, we apply the tensile load on the [001]-oriented pristine Cu NWs of three different diameters and their oxidized counterparts (core/shell Cu/Cu$_x$O$_y$ structure) at a constant strain rate of 1×10^{-8} (0.01% ps^{-1}) at 300 K. Periodic boundary conditions are applied in the axial direction. Resulting engineering stresses and strains are monitored throughout the applied external tensile mechanical loading. Furthermore, the pristine Cu NWs have been taken as the reference for further comparing the influence of a pre-existing oxide shell layer on the mechanical tensile properties and the deformation mechanism of NWs.

Figure 7 shows the influence of size on the representative engineering stress–strain responses of the pristine and oxidized Cu NWs under the external constant applied tension load. The engineering stress–strain profile of the pristine NWs of various diameters shows similar behavior in the elastic regime with sharp drops of the flow stress, but differences are observed in the plastic deformation region, as seen in Fig. 7(a). The yield stress and strain of the pristine NWs are slightly size dependent, such as a slight increase in the yield stress and strain from 13.30 GPa at a strain value of 11.07% to 14.52 GPa at a strain value of 11.12%, respectively, as the radius of NW increased from $\sim$2.08 to $\sim$5.20 nm. Young's modulus of the pristine NWs is decreased as the radius decreases, as seen in Table I. The pristine NWs possess relatively less structural defects at the surface that lead insignificant size effects on the yield strain

during tensile loading except for a slight increase in the yield stress. In smaller radius cases, the nucleation of initial dislocations from the pristine NW surfaces is requiring relatively low stresses to onset tensile plasticity. Thus, the strength of NWs increases slightly with increasing diameter, which is mainly attributed to the free surface effects. This suggests that surface defects do not play a significant role in the yield behavior and nucleation of the initial partial dislocation of the pristine NWs, contrary to their oxidized counterparts.

The representative engineering stress–strain curves of the oxidized NW show linear behavior in the elastic regime but relatively more extreme in the plastic deformation region and similarly the pristine counterparts, as seen in Fig. 7(b). In addition to that, it shows significantly different behavior, particularly revealing that the oxidized NWs with the smallest diameter possess a lower yield stress and strain to onset plasticity and lower elastic elongation. The unique pre-existing oxide layer structure accelerates the onset of plasticity and strongly influences the tensile mechanical properties of the NW, especially for the oxidized NW with the smaller diameters. Young's moduli are decreased as the radius of oxidized NWs decreases, confirming the importance of the pre-existing oxide shell layer on the tensile mechanical properties of Cu NW as the size of the NWs gets smaller, as seen in Table I. The yield stress, e.g., the elastic–plastic mode transition, depends significantly on the diameter and also on the pre-existing oxide layer, surface stress, and defects. Interestingly, our result clearly indicates that the strength, yield stress and strain, and Young's modulus of the oxidized NW with a radius of $\sim$2.35 nm is significantly lower than that of oxidized NWs (the other two bigger diameters). Specifically, the oxidized NW with a radius of $\sim$2.35 easily activates defects to the onset plasticity to relieve the elastic straining energy of the NWs and show a significant drop in the peak stress as compared with their counterparts. In particular, the smaller oxidized NW possesses relatively higher surface defects and complex interplay between oxide defects and a metallic core that lead strong size effects on the yield stress of NWs. Interestingly, the oxidized NW with a radius of $\sim$3.30 fails at $\sim$19% of strain.

It is interesting to compare qualitatively the mechanical properties of both the pristine Cu NW and its oxidized counterpart. The qualitative comparison and analysis of the corresponding engineering stress–strain curves provide a deeper understanding of the role of the size and the pre-oxide shell layer on the tensile deformation mechanism and related properties. We observe a similar trend as reported in other studies for the tensile stress–strain curves of both the pristine Cu NWs and their oxide counterparts that reveals approximately linear elastic behavior up to the yield strain and ends with a rapid drop in the flow stresses to onset plasticity.[8] This indicates the ending of the elastic deformation and consequent plastic deformation as a result of initiation (emitted) of defects and their motion within the NW during straining. The plastic deformation is followed immediately by initiation of dislocations around the NW's free surface or the oxidized layer. The onset of plasticity leads to a rapid release of significant elastic strain energy accumulation in the crystal lattice and, thus, a rapid relieve of tensile stress, e.g., a significant stress drop in the flow stress. Soon after the onset of plasticity, defect interactions within the NW volume change the tensile deformation response from linear to saw-toothed or zigzag of stress–strain behavior.

03 July 2023 12:42:10
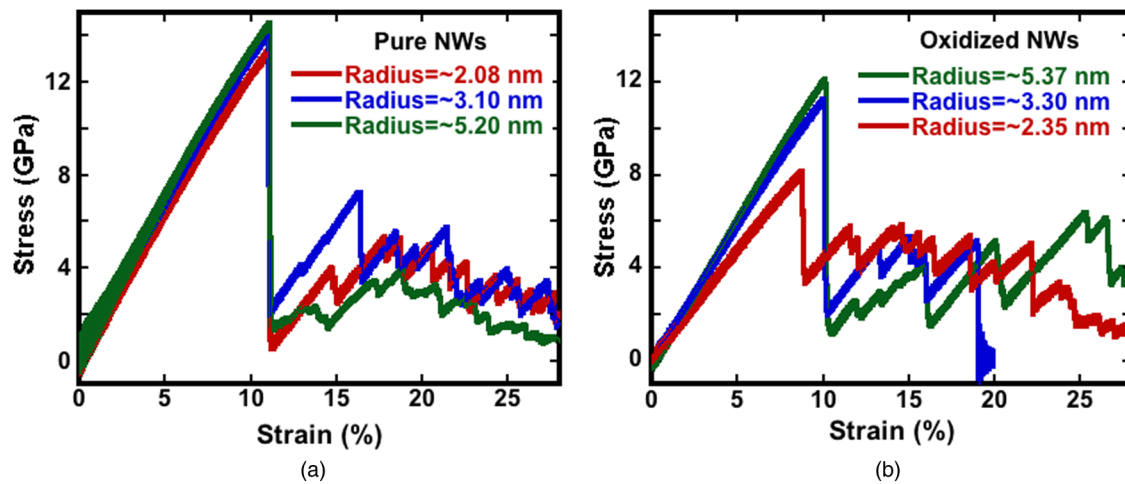
FIG. 7. Shows the quantitative comparison of the engineering tensile stress–strain curve in between the pristine NWs (a) and also (b) their corresponding oxidized counterparts. The engineering stress–strain curves indicate the pre-existing oxide layer effect in the yield stress and strain. The deformation behavior of pristine NWs looks like quite similar to each other in the elastic regime, but the plastic regime is significantly different.

The mechanical behavior of the crystalline core/oxide shell (Cu/Cu_xO_y) hetero-structured NW significantly differs from its pristine counterpart, suggesting that the formation of an oxide Cu_xO_y shell layer with defects is also notably different from each other. The complex interaction and interplay between the metallic Cu core and the oxidized Cu_xO_y shell (e.g., Cu–O interaction in the oxide shell layer) affect the overall qualitative mechanical behavior and properties of the NWs. For example, Young's modulus values of the pristine NWs with radii of ~2.08, ~3.10, and ~5.20 nm are 123.5, 131.5, and 135.8 GPa, and the corresponding values for their oxidized counterparts are 93.6, 114.3, and 120.3 GPa, respectively, indicating significant variations in Young's modulus with the size and the pre-existing oxide layer. The calculated Young's modulus of the pristine NWs is ~24.3, ~13.1, and ~11.4% higher than their corresponding oxidized counterparts in the increasing order of size, respectively. Also, Young's modulus reduces with the reduction in the diameter of the NWs. The average tensile yield stress values for the pristine NWs as increasing order of sizes are 13.30, 14.05, and 14.52 GPa, respectively, and their corresponding strain values are 11.07%, 11.05%, and 11.12%. Similarly, the yield stresses of the

oxidized NWs are 8.10, 11.23, and 12.10 GPa, respectively, and the corresponding values for their strain values are 8.78%, 10.08%, and 10.13%. The tensile yield stress of the pristine NWs is ~39.5%, ~20.1%, and ~16.7%, much higher than their corresponding oxidized counterparts' increasing order of size, respectively, and, hence, in the NW with and without the pre-existing oxide layer, the initial dislocations around the free surface at different yield stress and strain values. Thus, the mechanical properties of the oxidized NW, such as both the yield stress and Young's modulus, are quite different from that of the pristine counterpart, suggesting that pre-existence of the oxide shell strongly influences the mechanical behavior and related properties of Cu NWs. Intuitively, the pre-existence of the oxide layer, including coupling effects from the resulting interfaces with the metallic core and defects around the free surface of the NW, may be the probable main reason for weakening of the Cu NWs, accelerating the onset of plasticity with lowering the elastic deformation range.

The sizes, shapes, orientations, pre-existing defects, temperatures, grain size, and various applied load and strain rates dependent on the mechanical properties and deformation behaviors of

TABLE I. The variations in yield strain (ϵ_z), yield stress (σ_z), and Young's modulus (E) of the pristine NWs with three different radii: 2.08, 3.10, and 5.20 nm and their oxidized counterparts at a constant strain rate of $10^8\,s^{-1}$ are shown. The values of the thickness of the resulting oxide shell layer (thickness) on each NW surface are also shown. These evaluated tensile mechanical properties of the oxidized Cu NWs are quite different from their pristine counterparts.

Radius of NW (nm)	Oxide shell layer thickness (nm)	ϵ_z (%)	σ_z (GPa)	E (GPa)
Pure = 2.08		11.07	13.30	123.5
Pure = 3.10		11.05	14.05	131.5
Pure = 5.20		11.12	14.52	135.8
Oxidized = 2.35	~0.343	8.78	8.10	93.6
Oxidized = 3.30	~0.219	10.08	11.23	114.3
Oxidized = 5.37	~0.179	10.13	12.10	120.3

pristine Cu NWs have been extensively investigated through atomistic simulations and experiments. Their corresponding works have derived some conclusions for the mechanical properties of the Cu NWs as well as elucidated the mechanical deformation behaviors of the Cu NWs. For example, Li *et al.* carried out MD simulations to investigate quantitatively the mechanical properties of the rectangular parallelepiped shape of [001]-oriented Cu NWs and their irradiation with energetic ion counterparts under both tension and compression.[10] The ion irradiation with using different energetic ions induces mainly two kinds of defects in the Cu NWs, namely, point defects (vacancies, interstitials, and ad-atoms) and stacking faults that soften the NWs. They revealed that induced defects types depend on the incident ion energy that influence on the overall mechanical properties of the Cu NWs. For example, the irradiated NWs exhibit to have smaller yield strain and stress and also a smaller Young modulus, compared with the pristine counterparts due to surface defect advancement in the nucleation of the partial dislocation to onset the plasticity. Likewise, as in our result, they observed that the stress–strain curves increases linearly in the elastic regime for the Cu NWs with and without irradiation.

Ji and Park performed MD simulations with embedded-atom-method (EAM) potential to investigate the coupled effects of different cross-sectional geometries, in particular, square and rectangular cross-sectional shapes and various free surface side orientation on the tensile mechanical behavior and properties of both [100] and [110]-oriented Cu NWs, respectively.[7] They demonstrated that the effects of cross-sectional geometry associated with different multiple surface facets of different size and orientation lead to the different deformation mechanism and the significant disparities in mechanical properties of the Cu NW, such as in yield stress and strain, fracture strain, and toughness of the Cu NWs. The square and rectangular cross-sectional form of [100]-oriented Cu NWs with {110} surfaces yield at 12.6 and 9 GPa, respectively. Moreover, they observed a brittle fracture around ∼30.0% for both square and rectangular Cu NWs, which is similar to our oxidized Cu NW with a radius of ∼3.10 nm that exhibits a brittle fracture around ∼20.0%.

Cao *et al.* investigated grain boundary (GB) effects on the strength and ductility of bamboo like polycrystalline metallic Cu NWs with a square cross section, including plastic deformation behavior and fracture mechanisms by using MD simulations based on EAM potential.[42] They demonstrate that polycrystalline Cu NWs with nanoscale grains exhibit tensile deformation behavior distinctly different from their [100] single-crystalline counterparts with a square cross section with {100} side surfaces. The nanoscale grain boundary regions associated with a heterogeneous structure in the metallic Cu NWs act as a potential source of dislocation emission, leading to quite different mechanical properties and behavior from single crystal counterparts, such as lowering the yield stress and the fracture strain of the polycrystalline NWs. The different dislocation emission mechanisms from grain boundaries rather than from free surfaces are responsible for the different yields and flow behavior of the two types of Cu NWs, playing a significant role in controlling both inelastic deformation and fracture processes in the Cu NWs. The overall competition between dislocation nucleation from GBs and from free surfaces is controlling the

yielding and mediating plastic deformation mechanisms of the NWs with GBs. They observed the NW linear stress–strain response during the elastic deformation.

Wu *et al.* performed large-scale MD simulations to study nanostructure and surface effects on the yield of Cu NWs of an identical dimension with four distinct nanostructures: polycrystalline nanocrystal (NC), nanotwinned single crystal (NTSC), single crystal (SC), and nanotwinned polycrystalline nanocrystal (NTNC) NWs, including the identification of corresponding yield mechanisms.[9] In fact, their simulations highlight that the yield strengths of Cu NWs are highly sensitive to their internal and surface structures, including that the difference of mechanical properties associated with the nanostructural features derive from which dislocations nucleate; e.g., nanostructural feature controls the yield behavior of all Cu NWs. Particularly, both surface defects and grain boundary triple junctions serve relatively as effective stress concentrators in reducing the yield stress of Cu NWs to onset plasticity, e.g., the macroscopic load required to nucleate initial dislocations, strongly suggesting that dislocation nucleation from these stress concentrators is probably the mechanism controlling the yield behavior of Cu NWs. In the case of SC and NTSC NWs, the initial yields occur via dislocation nucleation from surfaces or surface defects, while NC and NTNC NWs yield via dislocation nucleation from grain boundary triple junctions. Importantly, the NC and NTNC Cu NWs are weaker than the SC and NTSC Cu NWs due to a greater number of triple junctions than surface defects within the NWs.

Sainath *et al.* performed MD simulations based on the EAM potential for the interaction between Cu atoms to study the size-dependent tensile deformation behavior of [100]-oriented Cu NWs as a function of square cross-sectional width (0.723–43.38 nm) with a fixed length of 21.69 nm at a constant strain rate of $1 \times 10^9 \, s^{-1}$ at 10 K.[8] They observed that the NWs exhibited linear elastic deformation followed by an abrupt drop in the flow stress. Also, the yield strength depends on the cross section of NWs. Both Young's modulus and yield strength exhibited a rapid decrease at small size NWs followed by a gradual decrease to saturation at a larger size. Similarly, Rohith *et al.* studied the effects of size (∼1.4 to ∼43.3 nm), temperature (10–700 K), and strain rate ($5 \times 10^7 \, s^{-1}$– $1 \times 10^9 \, s^{-1}$) on variations in the dislocation density and deformation mechanisms in [100]-oriented Cu NWs.[43] They concluded that the rate of dislocation exhaustion strongly depends on these three parameters. Specifically, the rate of dislocation exhaustion increases with increasing strain rate and increasing temperature, but with decreasing size.

Skarlinski and Quesnel performed reactive MD simulations based on charge-optimized many body potentials (COMBs) to investigate the effects of pre-existing native oxide layers on the tensile mechanical properties of a Cu thin film. Particularly, they studied yield stress, the Young modulus, and failure mechanisms by applying various applied strain rates, different temperatures, and oxide shell layer thicknesses.[17] They reported that the native oxide layer strongly affects the tensile mechanical properties of the Cu thin film, reducing the activation volume for yielding. Similarly, in our results, the NWs exhibit the apparent stress–strain linearity in the elastic regime. Furthermore, the pre-existing oxide layer leads significantly to the decreased Young's modulus, yield stress and the

embrittlement of samples. Specifically, the oxide-coated Cu films are considerably less ductile than the pristine counterparts. Also, the formed thin oxide layers on the Cu thin film have an amorphous structure with a mixture of Cu_2O and CuO structures.

Gu and Zhan investigated the tensile properties of single-crystalline rectangular Cu NW with and without different kinds of surface defects under varying temperatures, strain rates, and sizes using EAM potential developed.[44] In particular, they systematically studied the surface defects on NWs in considering different defect orientations and distributions. Importantly, their results revealed that the surface defects play a decisive role on the mechanical tensile properties of Cu NWs, such as a dislocation source during the applied deformation process. The pre-existing different surface defects on the NWs lead to a significant decrease in the yield stress and strain as compared with the pristine counterparts. The yield strength is highly dependent on the applied strain rate. They indicated that Young's modulus is insensitive of surface defects and also independent of the strain rate. In addition to that, Young's modulus is decreased as temperature increases. Similarly to our results, they also observed almost linear stress–strain curves of all NWs in the elastic regime and a saw-toothed shape in the plastic regime.

Overall, the pristine NWs with and without a pre-existing oxide shell layer mainly exhibit quite a different mechanical deformation mechanism and properties that are originated from free surfaces and an oxide layer for the pristine Cu NWs and their oxidized counterparts, respectively. The presence of the fraction of disordered (un-coordinated) atoms at the pristine NW surface and similarly the increased fraction of un-coordinated atoms that are positioned at the oxidize surface and interface are directly responsible for the nucleation of dislocations from the free surface and oxidized sources.[9,16] This is the origin of the much lower yield stress in the oxidized NWs. Our simulation results indicate that the yielding mechanism occurs via the first nucleation and propagation of partial dislocation from the pristine NW or its oxidized surfaces, affecting the overall deformation mechanism during the mechanical loading.[9] This intuitively suggests that initial dislocation nucleation from the free or oxidized surfaces is the mechanism to control the Cu NW yields and then mediate the overall deformation mechanism. In addition that, surface states of NWs, such as the initial atomic microstructure, initial defects, and flaws associated with the formation of a rough oxide layer and an interface between the metallic core and the oxide layer, the lattice mismatch between the Cu_xO_y shell and the metallic Cu core is directly responsible for the variation of mechanical properties and the dissimilarity of the stress–strain curves, such as the different yields and plastic flow behavior and dislocation nucleation mechanisms and also for the size dependence.[14,16,17,21] Specifically, competition between the two types of surface states, the free surfaces, and oxidized surfaces with the core structure play a dominant role in controlling the deformation mechanical behavior and mechanisms of NWs and dictate dislocation migration, at least for the NW sizes we simulated here. It is suggesting that the effects of a surface oxide layer on the yield behavior of the Cu NWs are very strong. Here, the O_2 molecules are locally reacted and incorporated consequently with the pristine NWs that is responsible for the formation and growth of the oxidation layer on the free surface NW, leading the drastic change in the local microstructure properties of the NWs and also promoting the formation of defects. As a result, the formation of an oxide shell layer creates an interface between the core and shell with defects and mismatches of atomistic arrangements that act relatively as nucleation sites for dislocations, lowering the tensile mechanical strain and stress to facilitate the onset of plastic deformation. In addition to that, the strong interaction between Cu and O atoms and/or the oxide defects and the metallic core in nano-scale NWs is also responsible to onset of first dislocations. In other words, in the oxidized NWs, both the free oxide surface and the interface are competing in controlling the plastic deformation. Importantly, atomistic simulations and experimental studies indicated that initial dislocations associated with the onset plasticity nucleate from the metallic and oxidized NW free surface due to the high surface-to-volume ratio resulting interfaces, defects, and flaws around the free surface of NW.[9,14,16,20,21] Generally, the size-dependent strength of metallic NWs (e.g., the onset of plasticity) is most likely associated with initial dislocation nucleation from the metallic and/or oxidized free surface. In particular, the resulting formation of the oxide layer on the NW surface leads significantly to induce the number of potential nucleation sites to initiation of defects for the onset plasticity. The pristine NWs have much less defects and the number of probable sites for initial defect nucleation to onset of plasticity than their oxidized counterparts and, thus, exhibit relatively high strength and yield stress and strain values contrary to the oxidized counterparts. According to previous studies, the mechanical properties of crystalline core/shell heterostructured NWs are affected by the dangling bonds, the disorder-induced distortions, and the lattice mismatch at the interface between the crystal core–amorphous shell structure, e.g., interface boundary effects that induce high intrinsic internal lattice stress coupled (induced) with the stress gradient at the core–shell interface region.[13,21]

D. Plastic deformation mechanism

The flow stress increases linearly with the applied external tensile strain in the elastic deformation regime. Meanwhile, there are no dislocations for all NWs, but there is a limited inhomogeneous crystal structure change from FCC to an unknown structure within the Cu NW based on defect evolution analysis using CNA. Also, just before the onset of plasticity, we observe limited inhomogeneous BCC phase transformation from an FCC structure mostly positioned around in the region close to the surface and the oxide layer region where significant stress concentration exists.[17] Overall, the Cu NWs maintain mostly their FCC structure in the elastic deformation region. Specifically, the tensile elastic strain is partially induced (mediated) by a crystal structure change from FCC to unknown (~0.7%) and BCC (~0.1%) within the all Cu NWs relative to their initial structures due to the redistribution of local intrinsic stresses.

Our observations reveal that the plasticity event is from the NW free surface and the oxide layer with the nucleation of defects (e.g., dislocations) with a hexagonal close packing (structure) atomic structure at a relatively high stress value, named as the yield stress and subsequent glided though the NW, leaving stacking faults behind. Importantly, the presence of an oxide layer on the
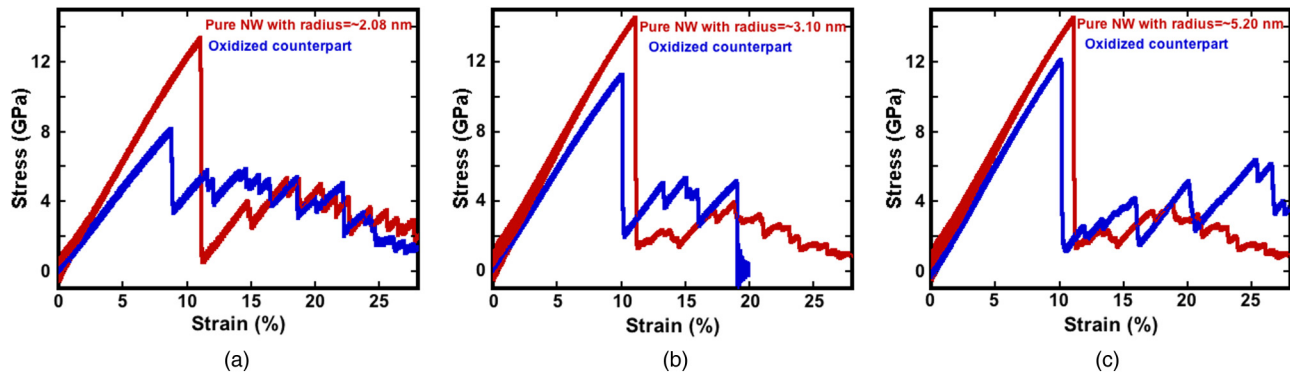
FIG. 8. Shows the quantitative comparison of the tensile engineering stress–strain curve in between (pair of) the pristine NWs and their pre-oxidized counterparts for the pristine NW radius (a) 2.08, (b) 3.10, and (c) 5.20 nm, respectively. It indicates that the pre-existing oxide layer effect is more significant on the yield stress and strain of the smallest diameter of NW. The oxidized Cu NW with the smallest diameter is easily deformed.

surface of the NWs facilitates initiation of initial dislocation from the locations of oxide defects to onset plasticity. The external applied tensile strain beyond the yield strain associated with relatively low stress leads directly to partial and collective dislocation activities within the NW's volume, changing the overall strain–stress deformation response pattern from linear to the saw-toothed (e.g., zigzag shape) of the stress–strain behavior. Specifically, the underlying plastic deformation mechanisms dynamically correlate with the consequence of the extensive individual and collective partial and full dislocation activities within the NW volume, such as the activation, annihilation, migration, development, propagation, and multiplication of defect activities, rotation of grains, twin generation, and nucleation of new multiple slip systems due to the redistribution of stresses because of local tensile stresses. Thus, the plastic deformation mechanism is more complex than the elastic one. Soon after the onset of plasticity, the defect processes, including a variety of dislocation–dislocation, dislocation–surfaces, and dislocation–stacking fault interactions, occur at a relatively very low-level stress value that consequently governs plastic deformation. Apart from having different yield stresses, the pristine NWs and their oxidized counterparts exhibit very different plastic deformation behavior, as shown in Fig. 8. For example, the oxide layer relatively raises the plastic flow stress as compared to their pristine counterparts.

According to Schmid's factors, nucleation and glide of dislocations are preferred sets of major {111} inclined slip planes in a subsequent plastic deformation process.[19,20,22] Likely, we observe that the dislocations within Cu NWs are favorably activated and glided on sets of the most favorable {111} inclined planes throughout the plastic deformation process. We observe many defect activation from a preferable nucleation site in the {111} crystallographic inclined slip planes within the largest-diameter NW with and without the oxide layer, which could lead to an increased higher probability of dislocation interactions to operate the tensile plastic relaxation mechanisms and consequently facilitate plastic deformations. Unlike the largest NW, the plastic deformations of the other NWs are associated with relatively less dislocations nucleation only

from a few sites within the NW. Thus, with decreasing size, the number of defect interactions is limited, leading to decrease ductility in the small size NWs. Importantly, the defect interactions allow the plastic relaxation mechanisms that eventually result in the annihilation of defects, making the smaller number of sources active and the tensile plastic deformation preferentially occur at some sites. It could be responsible for decreasing plastic flow stress and results in higher propensity to nucleate brittle-like fractures in smaller diameter NWs and finally shear failure in a gradual manner.

The NWs are continuously extended by these dislocation activities at the various relatively low plastic stress levels associated with the repeated rise and drop in the plastic flow stress, accommodating the applied external tensile load. Either of each individual and collective nucleation and multiplication of dislocations at new slip planes causes to sharply increase the flow stress after each drop in the plastic regime.[22] Similarly, the propagation of termination defects drops the flow stress to some extent. The plastic flow stress rise and drop that are caused by the tensile plastic deformation through defect activities and interactions are consistent with previous MD studies in Cu NW.[16,19,20] Importantly, the defect (dislocation–stacking fault) interactions eventually result in the annihilation of defects, such as stacking faults due to the redistribution of stresses because of local tensile stresses, corresponding to the following decreased plastic flow stress. We observe the obvious sample shape change, including the surface morphology and orientation of the NWs.

IV. CONCLUSION

Here, we study the influence of the pre-existing oxide layer and size on the tensile deformation behavior of [001]-oriented metallic Cu NWs under an applied constant tensile strain rate using ReaxFF MD simulation. We comprehensively quantify the extent to which the formation of an oxide shell layer modifies the mechanical deformation properties of the Cu NWs. Due to the pronounced surface effects caused by the formation of an oxide

03 July 2023 12:42:10

layer associated with a high surface-to-volume ratio, the mechanical behaviors of the oxidized Cu NWs significantly differ from their pristine counterparts. Our overall comparison of results between the pristine NWs and its oxide counterparts confirms that the presence of an oxide shell layer has a decisive role on the onset of plasticity and modulation of the overall tensile mechanical deformation mechanism and related properties of Cu NW, resulting in weakening the Cu NW. Our work also clarifies that an essential role of the pre-oxide shell layer at the free surface accelerates the initiation of defects to the onset of plastic plasticity. The oxidized NWs exhibit low yield stress and strain to the onset of plasticity and low elastic elongation (e.g., smaller elastic strain).

Thus, our computational MD study provides us deeper atomic-scale insights into the significance of a pre-existing oxide shell layer on mechanical properties of the Cu NWs. This knowledge, along with an understanding of the atomic-scale effects of the pre-existing oxide shell layer on the mechanical properties, can help engineers determine an acceptable limit for the surface oxide shell layer to avoid mechanical failure and effectively develop new functionality, desired mechanical properties with optimized performance, and enhanced reliability with Cu NW devices. Overall, it is worth noting that the existing of an oxide layer offers additional degrees of freedom in tuning the mechanical properties of NW.

ACKNOWLEDGMENTS

AUTHOR DECLARATIONS

Conflict of Interest

The authors have no conflicts to disclose.

Author Contributions

Gurcan Aral: Formal analysis (equal); Investigation (equal); Methodology (equal); Visualization (equal); Writing – original draft (equal). **Md Mahbubul Islam:** Writing – review & editing (equal).

DATA AVAILABILITY

The data that support the findings of this study are available from the corresponding author upon reasonable request.

REFERENCES

[1]B. Jeon, S. K. R. S. Sankaranarayanan, A. C. T. van Duin, and S. Ramanathan, Philos. Mag. **91**(32), 4073–4088 (2011).
[2]X. Li, Y. Wang, C. Yin, and Z. Yin, J. Mater. Chem. C **8**, 849–872 (2020).
[3]Z. C. S. Ye, I. E. Stewart, B. J. Wiley, and Z. Chen, ACS Nano **8**(9), 9673–9679 (2014).
[4]T. Ozkan, D. Shaddock, D. M. Lipkin, and I. Chasiotis, Mater. Res. Express **1**, 035020 (2014).
[5]Y. Unutulmazsoy, C. Cancellieri, M. Chiodi, S. Siol, L. Lin, and L. P. H. Jeurgens, J. Appl. Phys. **127**, 065101 (2020).
[6]L. Xu, Y. Yang, Z. W. Hu, and S. H. Yu, ACS Nano **10**, 3823–3834 (2016).
[7]C. Ji and H. S. Park, Nanotechnology **18**, 305704 (2007).
[8]G. Sainath, P. Rohith, and B. K. Choudhary, Philos. Mag. **91**(32), 4073–4088 (2011).
[9]Z. X. Wu, Y. W. Zhang, M. H. Jhon, J. R. Greer, and D. J. Srolovitz, Acta Mater. **61**, 1831–1842 (2013).
[10]W. Li, L. Sun, J. Xue, J. Wang, and H. Duan, Nucl. Instrum. Methods Phys. Res. B **307**, 158–164 (2013).
[11]A. Ahmed, P. Elvati, and A. Violi, RSC Adv. **5**, 35033 (2015).
[12]D. Mardiansyah, T. Badloe, K. Triyana, M. Q. Mehmood, N. R. Hosseini, Y. Lee, H. Sabarman, K. Kim, and J. Rho, Sci. Rep. **8**, 10639 (2018).
[13]X. Zhang, P. Zheng, Y. Ma, Y. Jiang, and H. Li, Mater. Des. **217**, 110605 (2022).
[14]G. F. Popovski, F. S. Ludwikowska, A. Köck, J. Keckes, and G. A. Maier, Sci. Rep. **9**, 807 (2019).
[15]X. Wang, R. Wang, H. Zhai, X. Shen, T. Wang, L. Shi, R. Yu, and J. Sun, ACS Appl. Mater. Interfaces **8**, 28831–28837 (2016).
[16]A. T. Jennings, J. Li, and J. R. Greer, Acta Mater. **59**, 5627–5637 (2011).
[17]M. D. Skarlinski and D. J. Quesnel, J. Appl. Phys. **118**, 235306 (2015).
[18]Y. Ma, X. Zhang, P. Zheng, E. Ni, Y. Wang, Y. Jiang, and H. Li, J. Phys. Chem. C **125**, 8759–8766 (2021).
[19]I. Salehinia and D. F. Bahr, Int. J. Plast. **52**, 133–146 (2014).
[20]D. Jang, C. Cai, and J. R. Greer, Nano Lett. **11**, 1743–1746 (2011).
[21]H. S. Park, K. Gall, and J. A. Zimmerman, J. Mech. Phys. Solids **54**, 1862–1881 (2006).
[22]A. Stukowski, Modell. Simul. Mater. Sci. Eng. **18**, 015012 (2010).
[23]M. P. Allen and L. J. Tildesley, *Computer Simulation of Liquids* (Oxford University Press, New York, 1987).
[24]G. J. Martyna, M. L. Klein, and M. Tuckerman, J. Chem. Phys. **97**, 2635 (1992).
[25]G. J. Martyna, D. J. Tobias, and M. L. Klein, J. Chem. Phys. **101**, 4177 (1994).
[26]G. Aral, Y. J. Wang, S. Ogata, and A. C. T. van Duin, J. Appl. Phys. **120**, 135104 (2016).
[27]G. Aral, J. Appl. Phys. **126**(13), 135109 (2019).
[28]G. Aral, M. M. Islam, Y. J. Wang, S. Ogata, and A. C. T. van Duin, Phys. Chem. Chem. Phys. **20**, 17289–17303 (2018).
[29]G. Aral, M. M. Islam, and A. C. T. van Duin, Phys. Chem. Chem. Phys. **20**(1), 284–298 (2018).
[30]G. Aral, M. M. Islam, Y. J. Wang, S. Ogata, and A. C. T. van Duin, J. Appl. Phys. **125**(16), 165102 (2019).
[31]G. Aral and M. M. Islam, New J. Chem. **45**(46), 21763–21774 (2021).
[32]F. G. Sen, A. T. Alpas, A. C. T. van Duin, and Y. Qi, Nat. Commun. **5**, 3959 (2014).
[33]F. G. Sen, Y. Qi, A. C. T. van Duin, and A. T. Alpas, Appl. Phys. Lett. **102**, 051912 (2013).
[34]K. I. Nomura, R. K. Kalia, A. Nakano, and P. Vashishta, Comput. Phys. Commun. **178**, 73–87 (2008).
[35]W. Zhu, H. Gong, Y. Han, M. Zhang, and A. C. T. van Duin, J. Phys. Chem. **124**, 12512–12520 (2020).
[36]S. Plimpton, J. Comput. Phys. **117**, 1–19 (1995).
[37]J. Leitner, D. Sedmidubský, M. Lojka, and O. Jankovský, Materials **13**, 2878 (2020).
[38]S. Jaatinen, J. Blomqvist, P. Salo, A. Puisto, M. Alatalo, M. Hirsimäki, M. Ahonen, and M. Valden, Phys. Rev. B **75**, 075402 (2007).
[39]H. Wu, S. R. Desai, and L. S. Wang, J. Phys. Chem. A **101**, 2103–2111 (1997).
[40]C. J. Cramer and W. B. Tolman, Acc. Chem. Res. **40**, 601–608 (2007).
[41]C. E. Elwell, N. L. Gagnon, B. D. Neisen, D. Dhar, A. D. Spaeth, G. M. Yee, and W. B. Tolman, Chem. Rev. **117**(3), 2059–2107 (2017).
[42]A. Cao, Y. Wei, and E. Ma, Phys. Rev. B: Condens. Matter **77**, 195429–192008 (2008).
[43]P. Rohith, G. Sainath, and V. S. Srinivasan, Phys. B **561**, 136–140 (2019).
[44]Y. T. Gu and H. F. Zhan, Int. J. Comput. Methods **09**(01), 1240003 (2012).

03 July 2023 12:42:10